Scientific Research Publishing

Energy and Power Engineering, 2022, 14, 680-704
https://www.scirp.org/journal/epe
ISSN Online: 1947-3818
ISSN Print: 1949-243X

Comparative Heat Transfer Data for Solid-Liquid Phase Change of D-Mannitol and Adipic Acid

Ulyana Horbatyuk, Ana Magalhães, Victor Ferreira, Carlos Pinho

CEFT, DEMEC, Faculty of Engineering, University of Porto, Porto, Portugal
Email: ctp@de.up.pt

How to cite this paper: Horbatyuk, U., Magalhães, A., Ferreira, V. and Pinho, C. (2022) Comparative Heat Transfer Data for Solid-Liquid Phase Change of D-Mannitol and Adipic Acid. *Energy and Power Engineering*, **14**, 680-704.
https://doi.org/10.4236/epe.2022.1411037

Received: July 26, 2022
Accepted: November 21, 2022
Published: November 24, 2022

Abstract

The goal of this work was to measure the heat transfer rates from thermofluid, Therminol 66, to two phase change materials, D-mannitol and adipic acid. It concerns the determination of heat transfer coefficients for the design of a concentrated solar energy plant requiring PCM thermal energy storage and is part of a wider set of experiments, where several PCMs were tested. An experimental installation was used with a cylindrical vessel with three tubes disposed almost horizontally (5˚ inclination), containing the phase change material, around which the thermal fluid flowed almost perpendicular to the tubes. The experimental installation allowed to recreate heating and cooling cycles. In order to evaluate the influence of the flow on the rate at which the heating and cooling processes took place, tests were performed at different thermofluid mass flow rates, concluding that there is no great influence, since the thermal resistance inside the tubes is much higher than on the outside. D-mannitol and adipic acid, present different phase change temperatures, 164˚C for D-mannitol and 152˚C for adipic acid. The average heat transfer coefficient, during the phase change process, was of 340 W/(m^{2}K) for D-mannitol and 1320 W/(m^{2}K) for adipic acid.

Keywords

Adipic Acid, D-Mannitol, Heat Transfer Coefficient, Phase Change Materials

1. Introduction

The use of phase change materials as a form of energy storage dates back to the 1970s, when they were used as thermal capacitors in lunar vehicles [1]. Phase change materials have been gaining significant importance in the world of tech-

nology, and in the world of thermal energy. Such importance is due to various reasons: the growing interest in the area of renewable energy, technological developments, and the demand for more and more comfort, among others [2] [3] [4] [5].

The use of phase change materials (PCMs) for thermal energy storage facilitates the use of solar systems even at low solar radiation periods, or the storage of surplus discarded thermal energy, available from any other type of source or plant [6] [7]. The greenhouse heating is a typical situation where this kind of energy storage is rather useful [8]. The application of PCMs in domestic heat water production from solar energy is another [9]. Sioshansi and Denholm [10] analyzed the economic impact of the introduction of a thermal energy storage system in concentrated solar energy plants, while Nithyanandam e Pitchumani [11] carried out a detailed economic analysis of the use of phase change materials in concentrated solar plants. The use of PCMs is an economic advantage as it reduces the number and size of the storage reservoirs [1]. It is a most promising solution because it allows a high storage density and an almost isothermal operation [12] [13]. There are many problems with the PCMs, namely due to their low thermal conductivities, low chemical stability, their corrosion capacity towards the storage reservoir materials and large volume variations associated to the change of phases. However, new technological developments on the synthesis of new materials are leading to new future promises [13].

The present study concerns the determination of heat transfer coefficients for the design of a concentrated solar energy plant requiring a PCM thermal energy storage. It is part of a wider set of experiments, where several PCMs were tested in order to obtain heat transfer values [14] [15] [16] [17].

2. Materials and Methods

2.1. Experimental Setup and Operating Procedure

The heating experiments for the phase change material (PCM) under study were carried out in a laboratory installation where hot thermal oil, the Therminol 66, transferred heat towards the PCM under analysis, which was placed inside a set of three transversal pipes with a slight slope to the horizontal. Two mass flow rates of the thermal oil were used in the experiments, according to the frequency of operation of the thermofluid circulating pump, namely 35 Hz and 50 Hz. During the PCM cooling period, the circulating thermofluid was cooled by a water cooled shell and tube heat exchanger. A quick reversal of the operating conditions of the laboratory set-up could easily be achieved, and the heating and cooling cycles of the PCM could be implemented in a straightforward manner. **Figure 1** presents a global scheme and a picture of the installation. During the PCM fusion process the thermofluid was heated in the heater A then it was pumped and sent to the test exchanger D. The Therminol 66 was chosen because it was intended to be used in a future solar plant operating with the PCMs under analysis.

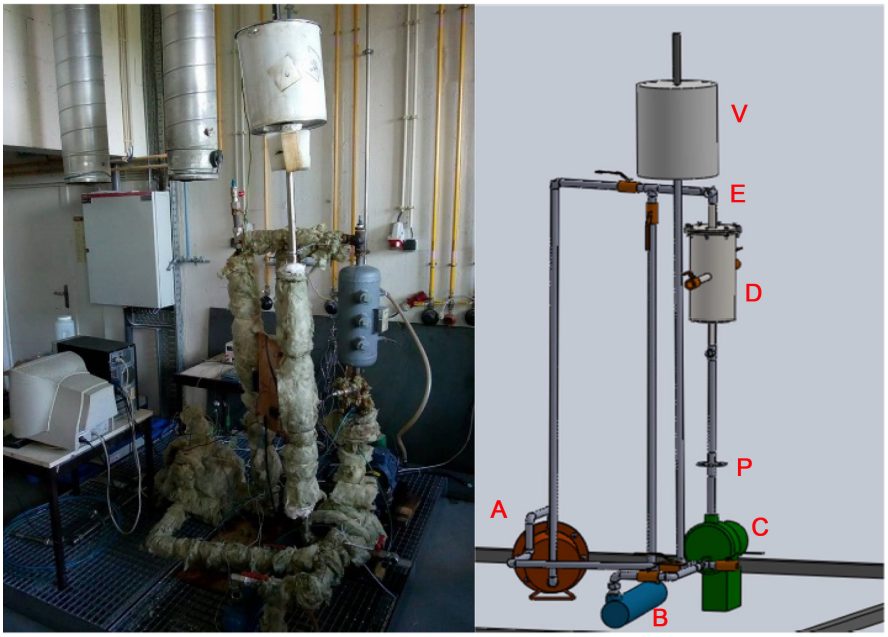

Figure 1. Picture (left) and scheme (right) of the experimental setup. A—Thermal oil electrical heater; B—Cooling heat exchanger; C—Centrifugal pump; D—Test heat exchanger; E—Air purge; P—Orifice plate flow meter; V—Expansion vessel.

During the PCM solidification step, the thermofluid was cooled in the shell and tube heat exchanger B and then pumped towards the test heat exchanger D. The mass flow rate of the thermofluid it was measured by the pressure drop through the orifice plate P, **Figure 1**. The laboratory installation was equipped with differential pressure transducers and T type thermocouples as necessary to follow the operating process. The computer based data acquisition system is composed by two USB connected interface boards from Measurement Computing and their operation was controlled by the DASYLab software.

The heat exchanger used in the experiments is composed by a single layer of three almost horizontal pipes. The heat exchanger is made of carbon steel with an internal diameter 159.3 mm and an external diameter of 168.3 mm. There is a bundle of three pipes, which will stay approximately in a perpendicular position towards the external thermal oil crossflow. These pipes have 210 mm length, 48.3 mm of external diameter and 43.1 mm of internal diameter. **Figure 2** presents a picture and 3D image of the heat exchanger while in **Figure 3** there is a 2D drawing. When installed in the experimental setup this heat exchanger is in a vertically position, **Figure 1**. In such situation, the transversal pipes have a 5˚ inclination towards the horizontal, to ease the PCM emptying process. The external heat transfer area of each pipe is around 0.0241 m^2 and the internal volume of pipe bundle is of 1.348 dm^3.

To evaluate the PCM temperature evolution during the heating and cooling phases, three T type thermocouples were placed inside each one of the pipes. The placement of each thermocouple is indicated by the red circle, **Figure 3**. Another thermocouple was placed attached to each pipe external wall, this

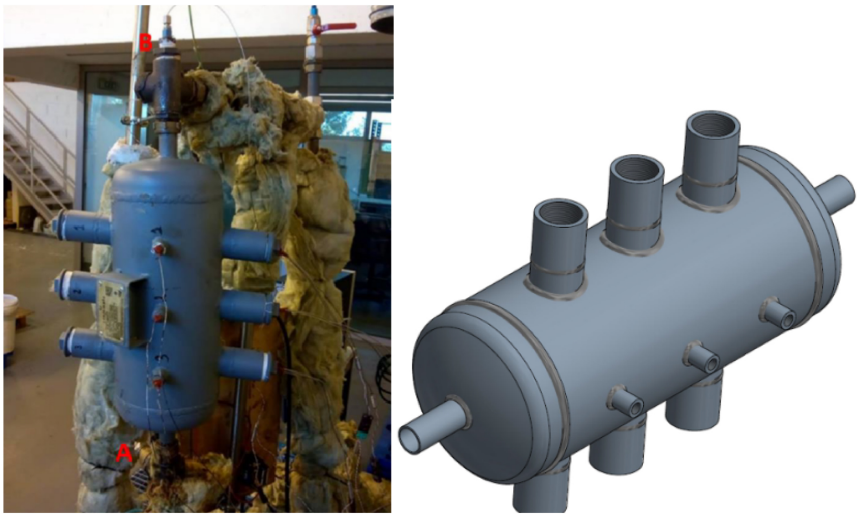

Figure 2. Picture and 3D image of the test heat exchanger.

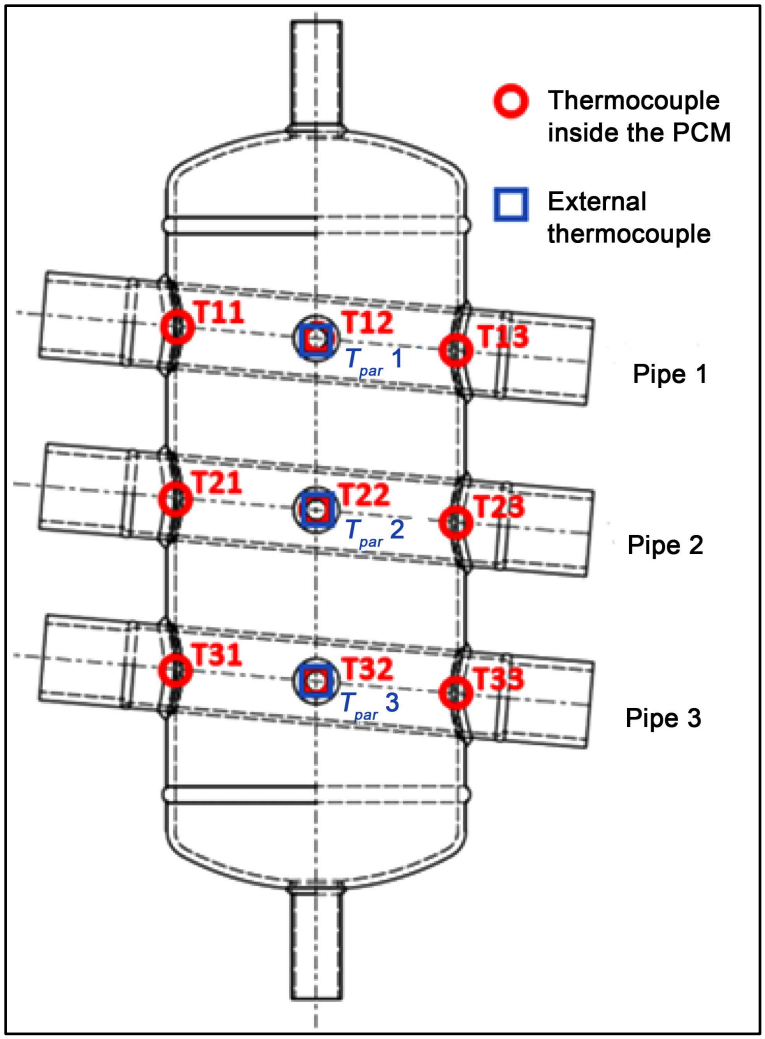

Figure 3. Test heat exchanger, in its vertical operating position, indicating the location of the inner (red circles) and outer (blue squares) thermocouples ($T_{par}1$, $T_{par}2$ and $T_{par}3$).

makes easier the determination of the external heat transfer coefficient from the thermal wall towards the pipe, inside which there is the PCM. The position of these external thermocouples is also indicated in Figure 3, by means of the blue squares. Two more T type thermocouples were placed at the heat exchanger inlet and outlet. In this way, the inlet and outlet temperatures of the thermal oil can be continuously monitored.

2.2. The Phase Change Materials

Two PCMs were studied. One has the commercial designation of Plus ICE A164, and is an alcoholic sugar derived from D-mannitol ($C_6H_{14}O_6$). The properties supplied by the manufacturer are presented in Table 1. Trhlikova *et al.* [18] carried out measurements of the thermal properties of this PCM through a ramp-wise and step-wise transient method, and some of the obtained properties are presented in Table 2, for three temperature values.

The D-mannitol is presented as white powder and its fusion temperature at 1 atm is about 168˚C. The D-mannitol is commonly used in the food and pharmaceutical industries and more recently, it was proposed as a thermal energy storage material [19] [20]. A total of 1.8 kg of PCM (PlusICEA164), equally distributed by the three pipes, was introduced inside the test heat exchanger. This corresponds to 522 kJ of latent heat of phase change.

Several authors have detected some problems on the D-mannitol usage as thermal energy storage material. Rodríguez-García *et al.* [21] indicate that there is a severe degradation of this material when working on thermal energy storage processes, while it is subjected to long stages above its fusion temperature. The clear phase change disappears and a vitreous transition phenomenon takes place and from a visual inspection of the degraded material it can be concluded that its solid structure is lost. It is replaced by a brownish pasty structure, typical of a caramelization process. Bayón and Rojas [22] also confirm the caramelization

Table 1. Properties of plus ICE A164 as supplied by the manufacturer.

Phase change temperature [˚C]	Density [kg/m^3]	Latent heat [kJ/kg]	Specific heat [kJ/(kg·K)]	Specific energy [MJ/m^3]
164	1500	290	2.42	435

Table 2. Some experimentally determined thermal properties of Plus ICE A164 [18].

Temperature [˚C]	Phase	Thermal diffusivity [mm^2/s]	Thermal conductivity [W/(m·K)]	Specific heat [kJ/(kg·K)]
30	Solid	0.054	0.06	0.68
100	Solid	0.049	0.18	2.45
260	Liquid	0.078	0.24	2.07

process and have identified a strong volatiles release followed by the polymerization of the solid material. These authors suggest that without a proper stabilization procedure of the material, either through encapsulation or through the formation of a composite structure, this material should not be used for thermal energy storage. Gasia *et al.* [23] have also detected a serious chemical and thermal degradation of the D-mannitol after a hundred operation cycles and consequently also refer that the D-mannitol should not be used as a thermal storage phase change material.

In spite of the above mentioned restrictions, that concern pure D-mannitol, and not commercially derived D-mannitol products, as is the present situation, the D-mannitol derivative under analysis is a product developed for thermal energy storage applications, and the expectancy is that it would not present such strong degradation of behavior and properties, as found in the pure material. Even so, industrial applications of D-mannitol derivatives must be carefully evaluated while the aging problems are not solved or minimized.

The second phase change material used in the experimental procedures was the adipic acid [23], **Table 3**. Adipic acid, also known as hexanedioic acid or 1.4-butanedicarboxylic acid, is a dicarboxylic acid. It has a melting point between 151˚C - 152˚C and its latent heat of fusion is between 213 and 275 kJ/kg [24]. It is a white, crystalline powder, soluble in water and organic solvents and odorless. It is used in a wide range of applications, however, almost 80 % of its production is for the production of polyamide. Other applications include plasticizers and lubricants, coatings, adhesives, and synthetic leather, among others. It was chosen for the present study, because it is the material that presents the best qualities after the D-mannitol, in the same average range of melting temperatures, and presents the advantage of not being so sensitive to the process of thermal aging, unlike D-mannitol.

Some studies have been carried out to determine the problems that arise due to the use of this material. The conclusions obtained after subjecting adipic acid to five heating and cooling cycles (between 40˚C - 200˚C) in an airtight container, its properties such as melting temperature and enthalpy of fusion did not change, but only an overcooling of approximately 5˚C occurred [25]. Another study, experimentally determined that no degradation occurs in the material when exposed to flowing air up to a temperature of 207˚C. The same study demonstrates through spectrometric analysis that there is no morphological change in adipic acid even after 100 cycles of heating and cooling between 150˚C - 200˚C.

Table 3. Properties of the adipic acid [26].

Phase change temperature [˚C]	Density [kg/m^3]	Latent heat [kJ/kg]	Specific heat [kJ/(kg K)]
151.5 - 153.0	1360 (solid at 20˚C) 1093 (liquid at 163˚C)	238.5	1.59 (solid at 20˚C) 2.26 (liquid at 150˚C)

However a reduction in the melting enthalpy of about 7% occurs, and a slight decrease in the solidification temperature, with the rest of the properties remaining unchanged [23].

This material is suitable for use in latent heat systems but it may present some corrosion problems when subjected to non-compatible vessels [27]. According to steel manufacturers, this material is compatible with an extensive range of stainless steels. Some manufacturers admit good compatibility with carbon steel, others assume corrosion.

Applying the first law of thermodynamics to the exchanger under study results that [14] [15],

$$\dot{Q} = \dot{m}c\left(T_{in} - T_{out}\right) \tag{1}$$

where $\dot{Q}$, $\dot{m}$ and c are the power delivered by the thermofluid in the test exchanger, the mass flow rate of the circulating thermofluid and the specific heat of the thermofluid, respectively. The temperatures T_{in} and T_{out} are the temperatures of the thermofluid at the inlet and outlet of the exchanger. The test exchanger is insulated, thus, all the power that is given off by the thermofluid is transferred to the phase change material,

$$\dot{Q} = UA\Delta T_{ml} \tag{2}$$

being ΔT_{ml} the log mean temperature difference.

Combining Equations (1) and (2) yields Equation (3), by which the overall heat transfer coefficient is calculated.

$$U = \frac{\dot{Q}}{A\Delta T_{ml}} = \frac{\dot{m}c\left(T_{in} - T_{out}\right)}{A\Delta T_{ml}} \tag{3}$$

In order to proceed with the calculation, it is necessary to know the value of the thermal power that the thermofluid gives in each instant, which is possible to do since in all tests the temperatures corresponding to the temperatures of the thermofluid at the inlet and outlet of the exchanger were recorded. The heat transfer area is the area of each tube, which is 0.0241 m^2.

Finally, the log mean temperature difference is calculated according to Equation (4) [14] [15]. This equation has this configuration because there is no flow within each tube. The PCM temperatures, T_{PCM}^{ini} and T_{PCM}^{fin}, are the initial and final temperatures, respectively.

$$\Delta T_{ml} = \frac{\left(T_{out} - T_{PCM}^{fin}\right) - \left(T_{in} - T_{PCM}^{ini}\right)}{\ln\left(\frac{T_{out} - T_{PCM}^{fin}}{T_{in} - T_{PCM}^{ini}}\right)} \tag{4}$$

To determine the heat transfer coefficient on the thermofluid side, the temperatures collected by the thermocouples near the outer walls of the tubes were used. Equation (5) [14] [15] was used for the calculation.

$$h_{ext} = \frac{\dot{Q}}{A_{ext}\left(T_{in} - T_{wall}\right)} \tag{5}$$

In this equation, $\dot{Q}$ represents the thermal power, A_{ext} is the external area of the tubes, T_{in} the inlet temperature of the thermofluid into the test exchanger, and T_{wall} is the wall temperature of the capsule.

The heat transfer coefficient in the phase change material is determined using Equation (6) [14] [15]. In this equation r_{ext} and r_{int} are the external and internal radius of the pipe containing the PCM, h_{ext} and h_{int} are the internal and external heat transfer coefficients and k is the thermal conductivity of the pipe material. Since the overall heat transfer coefficient U, and the thermofluid side heat transfer coefficient h_{ext} have already been determined, obtaining h_{int} is straightforward.

$$U = \left[\frac{r_{ext}}{r_{int} h_{int}} + \frac{r_{ext} \ln\left(\frac{r_{ext}}{r_{int}}\right)}{k} + \frac{1}{h_{ext}} \right]^{-1} \tag{6}$$

To analyze all the data, constant successive time intervals and average temperature values for these intervals were used along the experimental runs.

3. Results and Discussion

3.1. Experimental Results for D-Mannitol

D-mannitol tests were performed using pumping frequencies of 35 Hz and 50 Hz. Each test comprises a heating and a cooling process. The heating conditions were kept the same, the thermofluid temperature raised from 30˚C to 190˚C. The thermofluid cooling was done initially with a water flow rate of 5 l/min, and after 20 minutes, at 3 l/min. The thermofluid temperature dropped from 190˚C to 20˚C and extracted heat from the PCM. Information on the thermofluid temperature evolution can be found elsewhere [14] [15] [16] [17].

The total mass encapsulated in three tubes of the exchanger is 1.8 kg and is equally distributed over the three tubes. For this mass, the thermal energy absorbed and released in the phase change process by D-mannitol (h_{sl} = 290 kJ/kg) is 522 kJ.

Table 4 presents the average values of thermofluid mass flow rate for the two different motor supply frequencies, 35 Hz and 50 Hz. When the supply frequency is higher, the higher is the thermofluid flow rate. The thermofluid mass flow rate also varies with the test phase, being lower during cooling. The pressure drop during the cooling process is higher, due to the passage of the thermofluid through the shell and tubewater cooler and the cooling pipe, decreasing its mass flow rate. In all cases presented, the Reynolds number indicates laminar flow conditions for the thermofluid.

The heating and cooling curves obtained during the D-mannitol tests are presented below, showing the thermocouples measurements inside the PCM, as well as the temperature of the heat transfer fluid at the heat exchanger inlet. Figure 4 shows the evolution of the temperatures during the heating process, for the 50

Table 4. Average mass flow rate for the D-mannitol experiments.

Frequency [Hz]	Process	$\dot{m}$ [kg/s]	Re_D
35	Heating	0.364	621
	Cooling	0.239	89
	Slow cooling	0.228	49
50	Heating	0.349	960
	Cooling	0.351	123
	Slow cooling	0.347	70

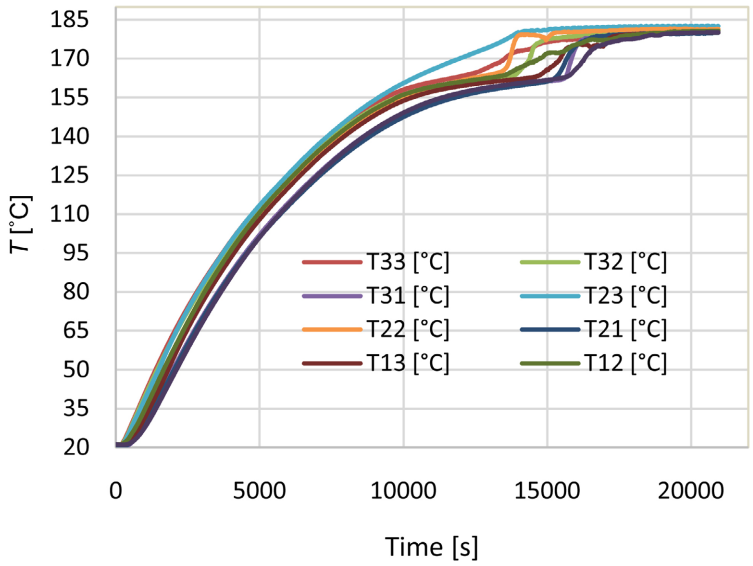

Figure 4. Temperature evolution over the D-mannitol heating. Thermofluid pump operating at 50 Hz.

Hz frequency of the thermofluid pump, while **Figure 5** and **Figure 6** show respectively the fast and the slower cooling curves.

The phase change within the three tubes, and within each tube, does not occur simultaneously, **Figure 4**. According to the results obtained, the first points where the phase change occurs are in tube 2, more precisely, the first thermocouple to detect the phase change is T21. This can be justified by the fact that heat transfer is increased due to the wake caused by tube 3, where the tube is located. Since thermocouple T21 is at a higher elevation within the tube, it may be the result of natural convection as the material melts near the walls of the tube, and consequently rises to the top, thus causing an increase in temperature. This is followed by the change in some parts of tube 3, as this is the tube that receives the first contact with the thermofluid, and finally, tube 1.

In tube 1, the first location where the phase change occurs is T12. Since this is in the central location of the tube, a possible justification is that there is greater flow stability of the thermofluid, which results in an equitable distribution of energy over the available heat transfer area.

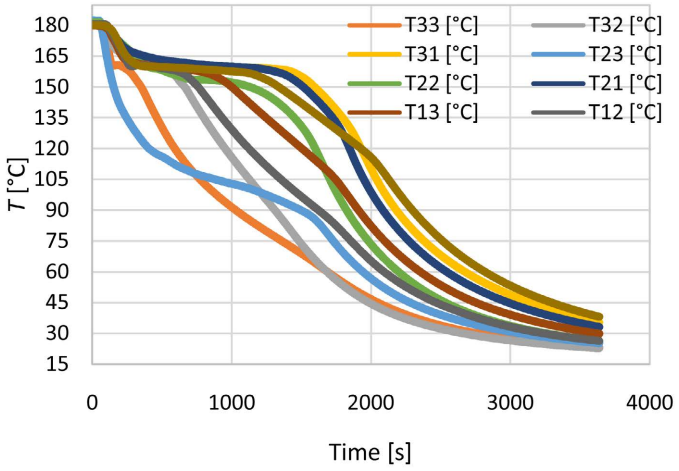

Figure 5. Temperature evolution over the D-mannitol cooling. Thermofluid pump at 50 Hz and cooling water flow rate of 5 l/min.

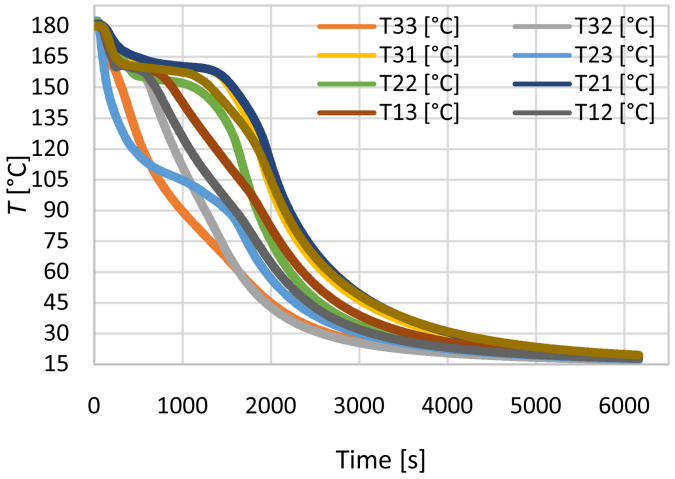

Figure 6. Temperature evolution over the D-mannitol slow cooling. Thermofluid pump at 50 Hz, initial cooling water flow rate of 5 l/min and subsequently of 3 l/min.

As far as cooling is concerned, Figure 5, the phase changes do not follow the same sequences as in heating, although the differences are only in the order of change in a few thermocouples. This may be caused by the reduced mass flow rate of the circulating thermofluid. Thus at the inlet of the test exchanger the jet effect is much smaller, affecting the heat exchange within it. The first thermocouple to detect the change is the T21 thermocouple, which is located in the center pipe of the exchanger. This is followed by the thermocouples in tubes 3 and 1, and the last thermocouple to record the change is thermocouple T13, which is located at a lower elevation of tube 1.

The cooling process is faster, since the power of the cooling exchanger (29 kW) used in the installation is much higher than the power of the heater (2 kW). It must be stressed that the pump frequency does not significantly affect the temperature evolutions, reason why only plots for a thermofluid pump frequen-

cy of 50 Hz are shown. Figure 6 shows the slow cooling process.

Figures 7-9 are the evolutions of the overall heat transfer coefficient U, the heat transfer coefficient inside the phase change material h_{int} and also the heat transfer coefficient on the thermofluid side h_{ext}. In order to calculate these parameters, Equations (1) to (4) were used.

Figure 7 shows the evolution of the overall heat transfer coefficient over the heating cycle. The overall heat transfer coefficient remains more or less constant, however there is a variation during the phase change and then increases again. This increase is due to convection effects taking phase in the melted material. On the other end, the overall heat transfer coefficient depends on the thermal conductivity of the phase change material, and it decreases with increasing temperature. However, the convection influence on the liquefied PCM is more important.

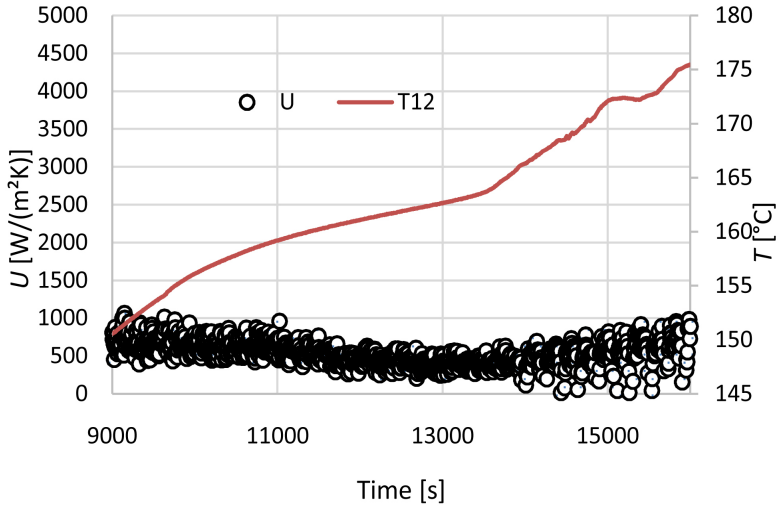

Figure 7. Overall heat transfer coefficient over the D-mannitol heating. Thermofluid pump operating at 50 Hz.

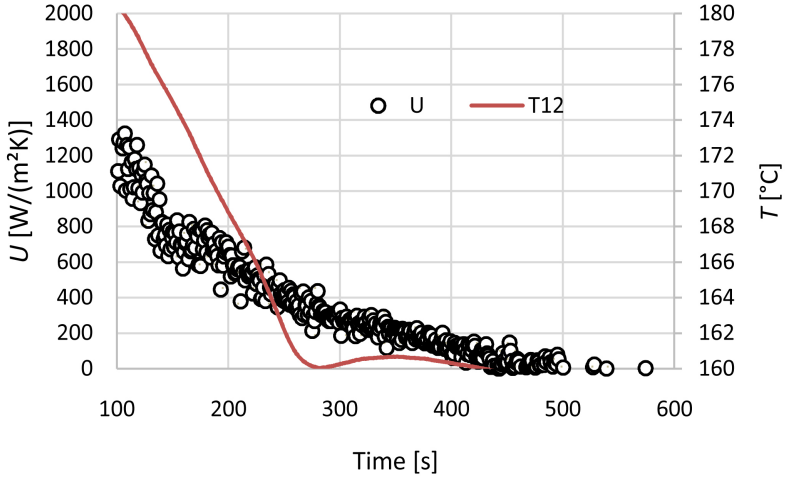

Figure 8. Overall heat transfer coefficient over the D-mannitol cooling. Thermofluid pump operating at 50 Hz. Cooling water mass flow rate of 5 l/min.

In the cooling process, Figure 8 and Figure 9, the overall heat transfer coefficient is highest at the beginning of the process, since the phase change material is molten and convection effects predominate. Thereafter this coefficient decreases and becomes almost constant. The slower cooling, Figure 9, does not show much difference from cooling at the rate of 5 l/min.

In Figures 7-9, the red line indicated by the reference T12 represents the time evolution of the PCM temperature measured with the thermocouple T12, as indicated in Figure 3. Information on the time evolution of the thermofluid temperature, at the entrance of the test heat exchanger, during the experiments, can be found elsewhere [17].

The average global heat transfer values for the D-mannitol experiments are shown in Table 5.

Figure 10 and Figure 11 show the evolutions obtained for tube 1 for the heating and cooling processes. As can be seen, this coefficient also presents some variation, however it follows a clear tendency to increase during the heating process and decrease during the cooling process. As already referred, two cooling processes were adopted. One with a constant flow rate for the cooling water at 5 l/s, and a slower cooling, starting with a cooling water flow rate of 5 l/s which, after about 20 min, was changed to 3 l/s. In Figure 12 this slower cooling can be observed and it is noticed that the process is a little more unstable than the faster cooling.

Figures 13-15 show the evolution of the heat transfer coefficient in the phase change material, in heating, cooling and slower cooling, respectively.

Table 5 shows the average values of the heat transfer coefficients ($\overline{U}$, $\overline{h}_{ext}$ and $\overline{h}_{int}$) for the D-mannitol experiments. These values comprise only the phase change interval.

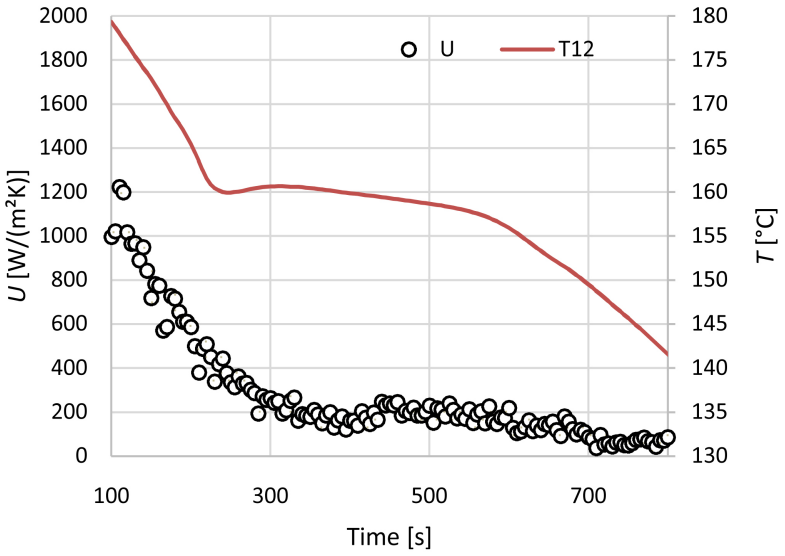

Figure 9. Overall heat transfer coefficient over the D-mannitol slow cooling. Thermofluid pump operating at 50 Hz. Cooling water mass flow rate of 5 l/min of during the first 20 minutes and 3 l/min afterwards.

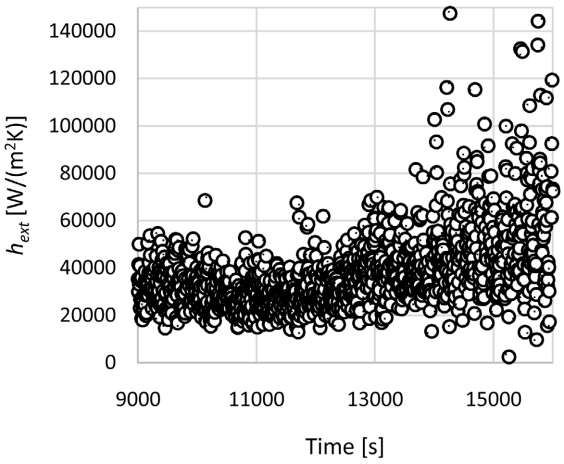

Figure 10. Heat transfer coefficient on the thermal oil side, over the D-mannitol heating. Thermofluid pump operating at 50 Hz.

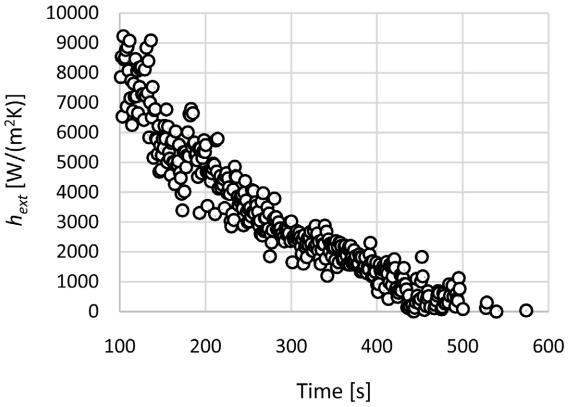

Figure 11. Heat transfer coefficient on the thermal oil side, over the D-mannitol heating. Thermofluid pump operating at 50 Hz.

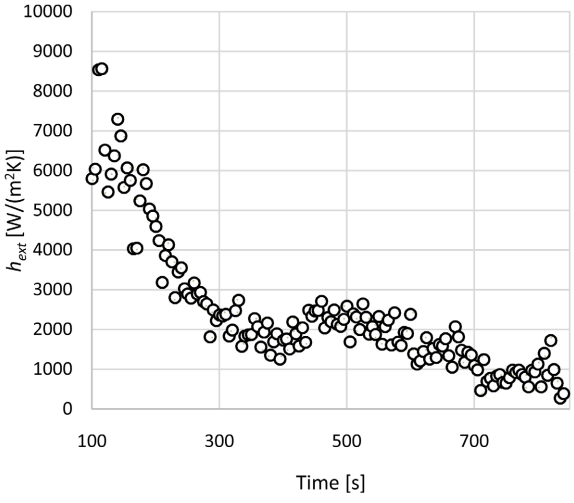

Figure 12. Heat transfer coefficient on the thermal oil side over the D-mannitol slow cooling. Thermofluid pump operating at 50 Hz. Cooling water mass flow rate of 5 l/min of during the first 20 minutes and 3 l/min afterwards.

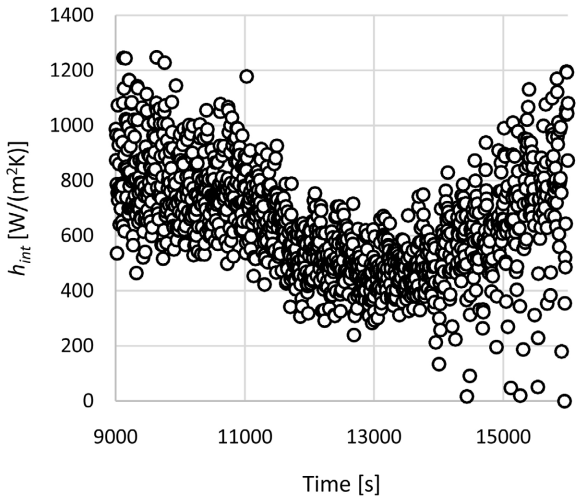

Figure 13. Heat transfer coefficient on the phase change material side, over the-D-mannitol heating. Thermofluid pump operating at 50 Hz.

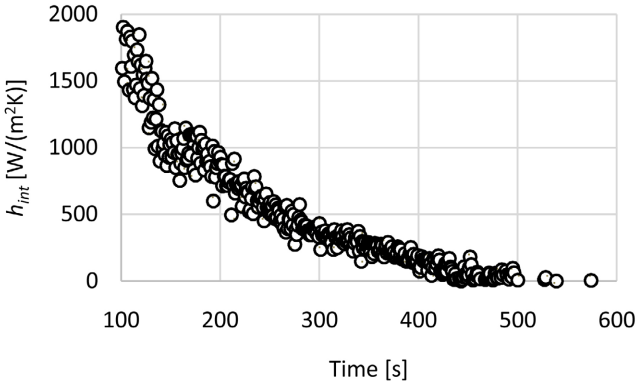

Figure 14. Heat transfer coefficient on the phase change material side over the D-mannitol cooling. Thermofluid pump operating at 50 Hz and 5 l/min of cooling water mass flow rate.

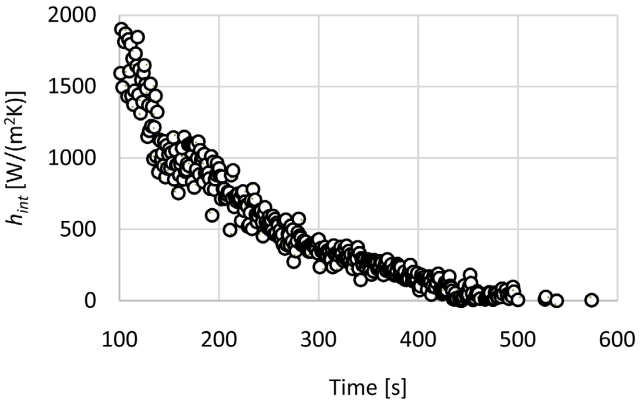

Figure 15. Heat transfer coefficient on the phase change material side over the D-mannitol slow cooling. Thermofluid pump operating at 50 Hz. Cooling water mass flow rate of 5 l/min of during the first 20 minutes and 3 l/min afterwards.

Table 5. Average values of heat transfer coefficients using D-mannitol.

Frequency [Hz]	Process	Pipe	$\bar{U}$ [W/(m²K)]	$\bar{h}_{ext}$ [W/(m²K)]	$\bar{h}_{int}$ [W/(m²K)]
35	Heating	1	192	6324	228
		2	331	49,741	385
		3	241	49,567	277
	Cooling	1	239	2117	314
		2	230	11,717	271
		3	239	13,281	252
	Slow cooling	1	225	1888	300
		2	212	7375	254
		3	234	7374	289
50	Heating	1	540	37,900	641
		2	265	175,799	306
		3	204	12,992	231
	Cooling	1	390	3219	451
		2	383	12,885	463
		3	399	12,885	484
	Slow cooling	1	271	2420	360
		2	265	16,828	317
		3	274	16,827	329

For D-mannitol the average value of the overall heat transfer obtained was 285 W/(m²K), for the heat transfer coefficient in the phase change material the obtained value was 340 W/(m²K) and for the heat transfer coefficient on the thermofluid side it was 24,507 W/(m²K). These values compare well with the equivalent values obtained by Rocha *et al.* [17], for the same PCM.

3.2. Experimental Results for Adipic Acid

The total mass encapsulated in the exchanger three tubes is now 1.36 kg. This mass is equally distributed over the three tubes. For this mass, the thermal energy absorbed and released in the phase change process by adipic acid (h_{sl} = 275 kJ/kg) is 373 kJ.

As with D-mannitol, the experimental tests were run at two different motor pump frequencies, 35 Hz and 50 Hz. From **Table 6** it can be concluded that for a higher power supply frequency, the circulating flow rate is higher, as verified in the case of D-mannitol, and is also lower during the cooling process.

Similarly to the experiments with D-mannitol, tests comprising heating and

Table 6. Average mass flow rate for the adipic acid experiments.

Frequency [Hz]	Process	$\dot{m}$ [kg/s]	Re_D
35	Heating	0.367	643
	Cooling	0.226	81
	Slow cooling	0.297	98
50	Heating	0.472	722
	Cooling	0.380	112
	Slow cooling	0.365	110

cooling of adipic acid were performed. Thus, heating was always done at the same rate, while cooling in one trial was done at a rate of 5 l/min, and in another trial, after the initial 20 min at a rate of 5 l/min, it was changed to 3 l/min. The thermofluid operating temperature range for the heating and cooling tests were the same as for the D-mannitol.

Observing **Figure 16** below, which concerns the heating of adipic acid at a frequency of 50 Hz, one can see that the phase change occurs initially in tube 3, and the thermocouple that detects this change is T31, followed by tubes 2 and 1, at thermocouples in the same position, T21 and T11. Then the phase change occurs in the center of the heat exchanger, at thermocouples T32 and T22. The last thermocouple to detect the phase change is T23. In this situation, the phase changes occur first at position 1 of each tube, at the highest elevation, followed by the middle position, position 2 and finally at the lowest elevation, position 3.

For the cooling experiments, **Figure 17** and **Figure 18**, the sequence with which the phase change occurs in the different thermocouples is roughly the same. The first and last thermocouples to detect the change are also T31 and T23, respectively. In this situation, the phase changes also occur initially in position 1 of each tube, which corresponds to the thermocouples at the highest level of the test heat exchanger, always starting in tube 3, then in tube 2 and finally in tube 1. Then the same occurs in position two, also starting in tube 3, then 2 and 1. Finally, the phase change occurs in position 3, which corresponds to the lowest level of the heat exchanger. The first tube where the phase change occurs is tube 3, then tube 1 and finally tube 2.

When a slower cooling was performed, **Figure 18**, the phase changes do not occur in the same way. The first thermocouple to detect the change is T31, followed by T21, as in the cases analyzed above. Next comes thermocouple T32, and only then does the first change occurs in tube 1, at thermocouple T11. The last thermocouple to detect the phase change is T13.

Following the same logic used in the analysis of the D-mannitol tests, the heat transfer coefficients obtained are presented next. These are the overall heat transfer coefficient U, the heat transfer coefficient inside the adipic acid h_{inp}, and the heat transfer coefficient on the thermofluid side h_{ext}. The same considerations used previously for D-mannitol were adopted, and it is again assumed that

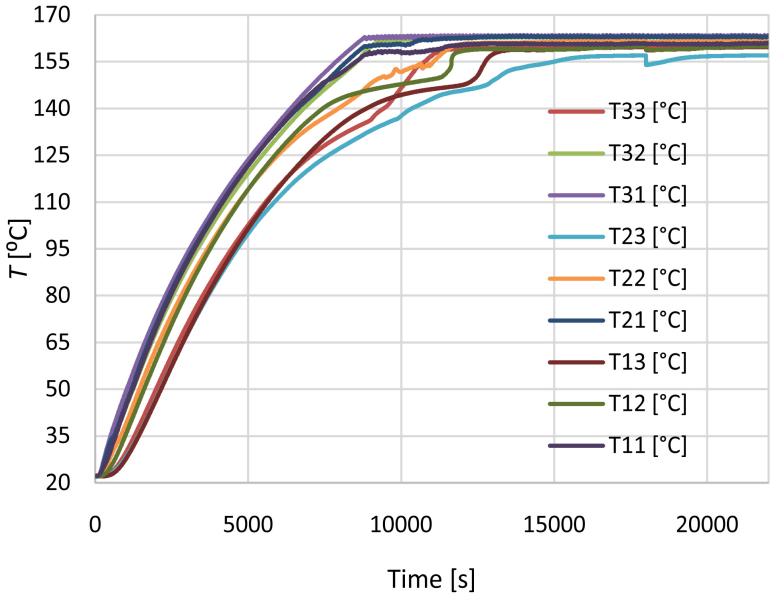

Figure 16. Temperature evolution for adipic acid heating. Thermofluid pump at 50 Hz.

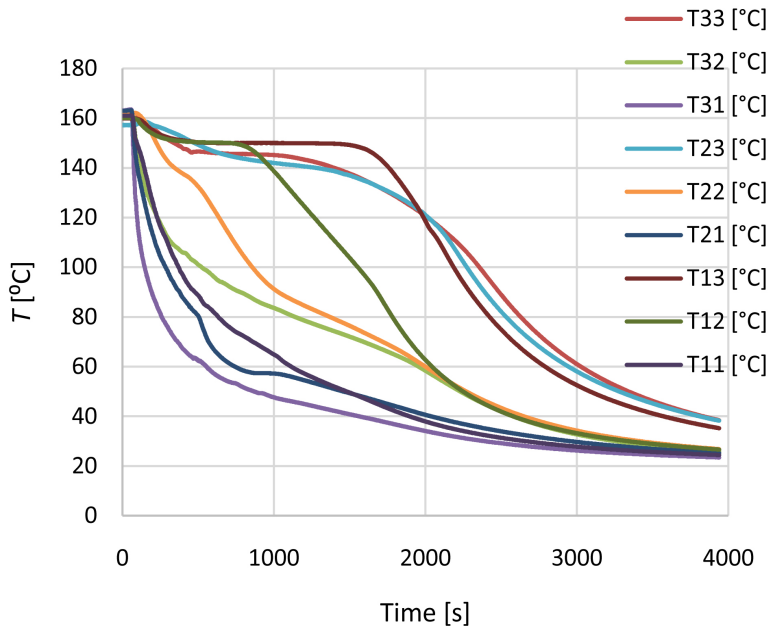

Figure 17. Temperature evolution over the adipic acid cooling. Thermofluid pump at 50 Hz. Cooling water flow rate of 5 l/min.

the heat energy transfer has a uniform distribution across the three tubes of the test exchanger.

The heat transfer coefficients were calculated based on the T12 thermocouple, as this is the thermocouple that is located in the center of the tube, and tube 1 is considered to be the location where the flow is the most stable. The external temperatures recorded by the thermocouple Tpar1, **Figure 3**, were considered the temperature at the wall of the tube.

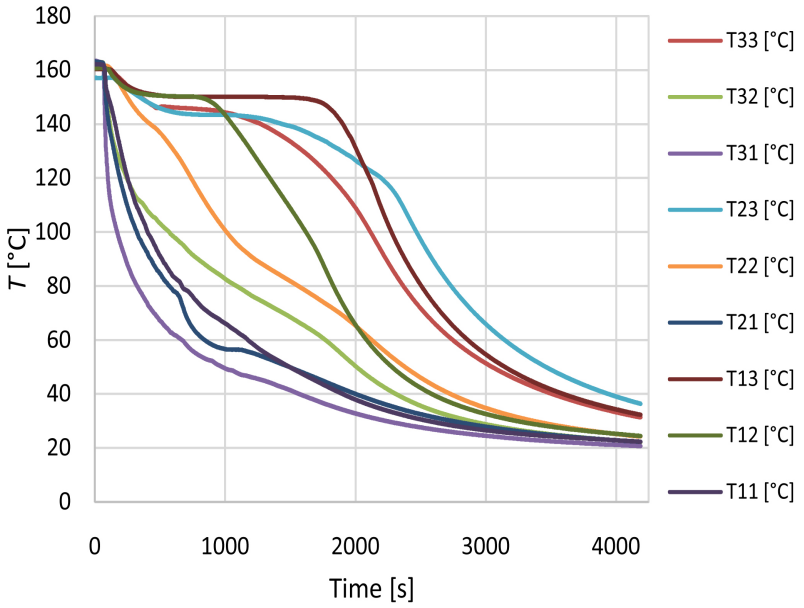

Figure 18. Temperature evolution over the adipic acid cooling. Thermofluid pump at 50 Hz. Cooling water flow rate of 5 l/min.

Figures 19-21 show the time evolution of the overall heat transfer coefficient *U*, for the heating and cooling phases.

Similarly as found for D-mannitol, the overall heat transfer coefficient decreases at the beginning of heating, Figure 19. Although there is no concrete data in the literature about the variation of the thermal conductivity coefficient of adipic acid, it can be admitted that a similar behavior is as seen in D-mannitol. Thus, it is concluded that there is a clear indication that the thermal conductivity of adipic acid, analogous to the case of D-mannitol, also decreases with increasing temperature. As the heating cycle proceeds, the overall heat transfer coefficient increases, as the effects of convection currents begin to predominate.

Regarding cooling, Figure 20 and Figure 21, the overall heat transfer coefficient shows high values since the material is in the liquid phase, and the effects of convection currents are noticeable. Beyond the point of phase change, the global heat transfer coefficient decreases and stabilizes

Figures 22-24 show the heat transfer coefficient evolution on the thermofluid side for a 50 Hz pump frequency. The data obtained in both heating and cooling show large variations, since the flow is irregular due to the impossibility of adding a stabilizing device, or increasing the inlet length of the test exchanger. It is observed, in the case of heating, that the trend of the heat transfer coefficient on the thermofluid side undergoes little change, remaining almost constant, Figure 22.

At the beginning of cooling, the heat transfer coefficient on the thermal fluid side is high. In both cases, the coefficient oscillates, becoming more pronounced for faster cooling, but in the final part of the cooling process it tends to remain constant, Figure 23 and Figure 24.

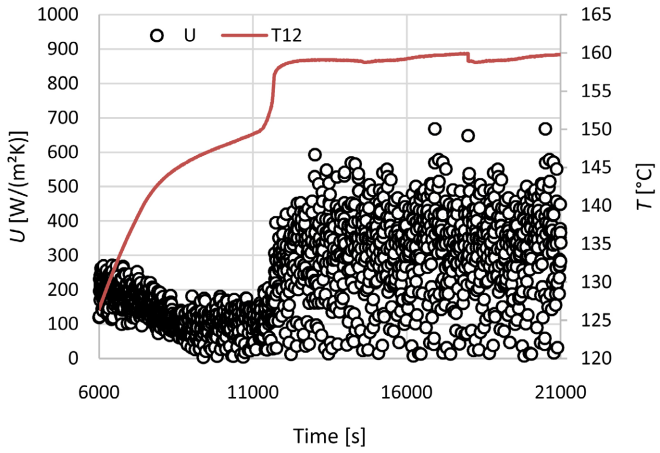

Figure 19. Overall heat transfer coefficient over the adipic acid heating. Thermofluid pump operating at 50 Hz.

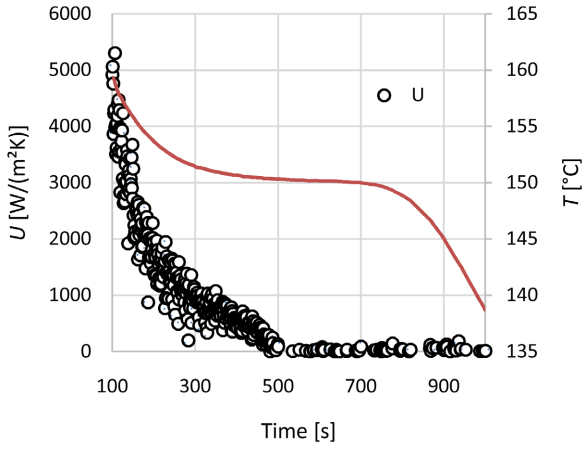

Figure 20. Overall heat transfer coefficient over the adipic acid cooling. Thermofluid pump operating at 50 Hz. Cooling water mass flow rate, 5 l/min.

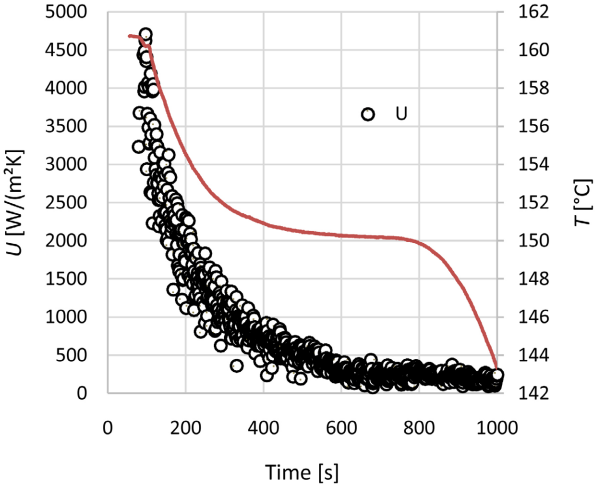

Figure 21. Overall heat transfer coefficient over the adipic acid slow cooling. Thermofluid pump operating at 50 Hz. Cooling water mass flow rate of 5 l/min during the first 20 minutes and 3 l/min afterwards.

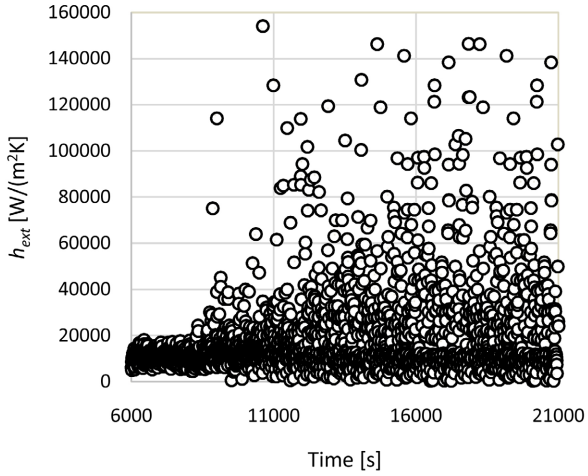

Figure 22. Heat transfer coefficient on the thermal oil side, over the adipic acid heating. Thermofluid pump operating at 50 Hz.

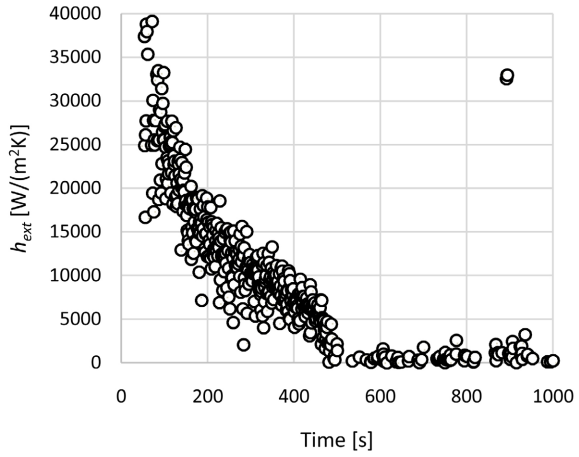

Figure 23. Heat transfer coefficient on the thermal oil side over the adipic acid cooling. Thermofluid pump operating at 50 Hz. Cooling water mass flow rate of 5 l/min.

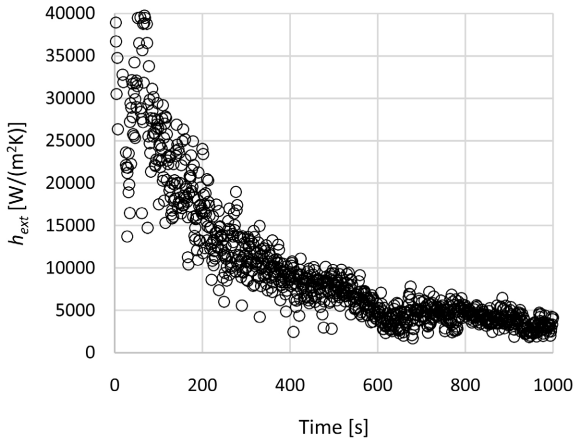

Figure 24. Heat transfer coefficient on the thermal oil side over the adipic acid slow cooling. Thermofluid pump operating at 50 Hz. Cooling water mass flow rate of 5 l/min during the first 20 minutes and 3 l/min afterwards.

Concerning the heat transfer coefficient in the phase change material, Figures 25-27, they present respectively the time evolution of this coefficient during heating, faster cooling and slower cooling.

Table 7 shows the average heat transfer coefficient values ($\overline{U}$, $\overline{h}_{ext}$ and $\overline{h}_{int}$) for adipic acid. These values are relative to the phase change interval.

From these adipic acid tests, the average value of the overall heat transfer obtained was 1008 W/(m^{2}K), of the heat transfer coefficient in the phase change material was 1320 W/(m^{2}K) and of the heat transfer coefficient on the thermofluid side was 38,720 W/(m^{2}K).

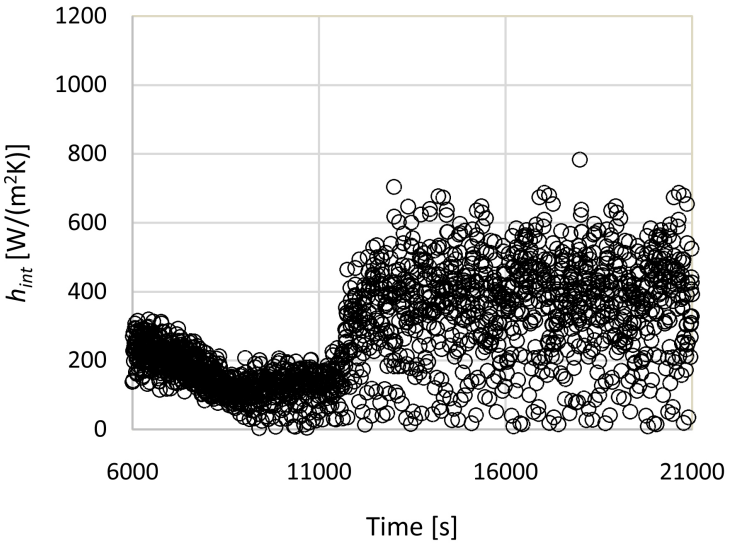

Figure 25. Heat transfer coefficient on the thermal oil side over the adipic acid heating Thermofluid pump operating at 50 Hz.

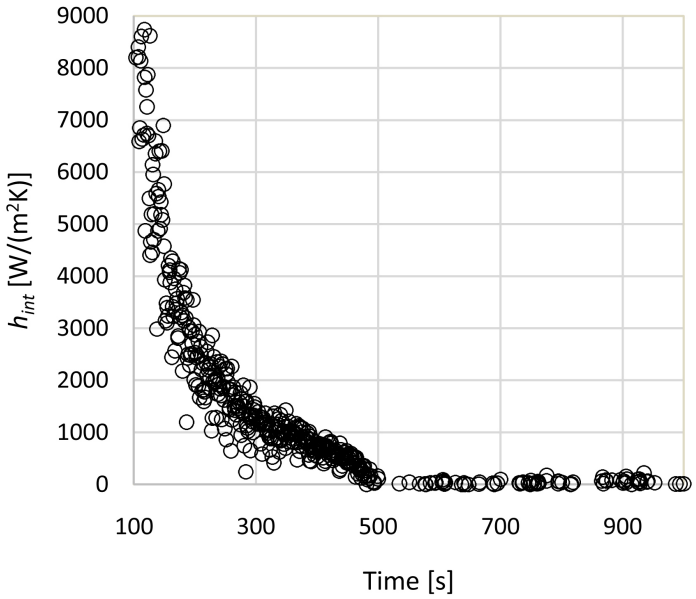

Figure 26. Heat transfer coefficient on the phase change material side over the adipic acid cooling. Thermofluid pump operating at 50 Hz. Cooling water mass flow rate of 5 l/min.

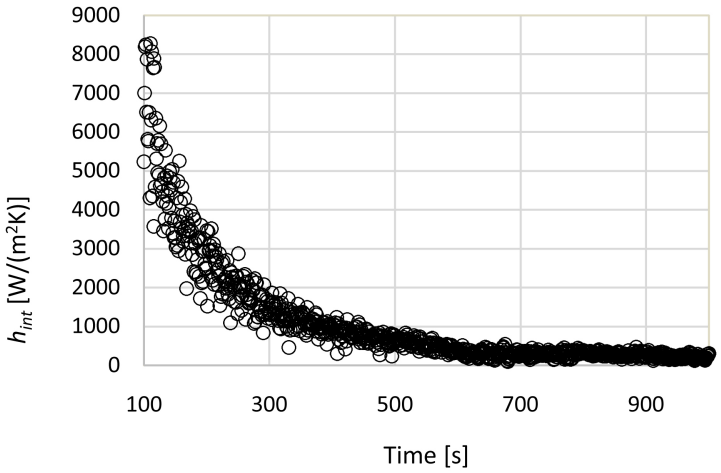

Figure 27. Heat transfer coefficient on the phase change material side over the adipic acid slow cooling. Thermofluid pump operating at 50 Hz. Cooling water mass flow rate of 5 l/min during the first 20 minutes and 3 l/min afterwards.

Table 7. Average values of heat transfer coefficients using adipic acid.

Frequency [Hz]	Process	Pipe	$\bar{U}$ [W/(m²K)]	$\bar{h}_{ext}$ [W/(m²K)]	$\bar{h}_{int}$ [W/(m²K)]
35	Heating	1	1114	32,814	1075
		2	1787	92,621	1815
		3	2699	92,621	3989
	Cooling	1	382	3470	547
		2	406	15,562	476
		3	609	19,288	910
	Slow cooling	1	337	3542	458
		2	393	28,661	539
		3	581	28,661	734
50	Heating	1	174	16,966	199
		2	271	33,867	312
		3	650	33,867	517
	Cooling	1	1446	16,259	2336
		2	1530	30,793	1963
		3	2234	44,549	3222
	Slow cooling	1	977	10,152	1150
		2	1028	71,063	1293
		3	1543	122,161	2174

4. Conclusions

The studied materials, D-mannitol and adipic acid, present different phase

change temperatures, namely 164˚C for D-mannitol and 152˚C for adipic acid. The facility available at the combustion laboratory of INEGI was used, which includes a test heat exchanger composed of a layer of three tubes, with an inclination of 5˚ with the horizontal, to ease up the PCM emptying procedure, where the phase change materials were inserted. Several heating/cooling cycles were performed in order to obtain heat transfer coefficients: overall, on the thermofluid side and finally in the phase change material.

When comparing the obtained values, the conclusion is that the heat transfer coefficients of adipic acid are much higher than those of D-mannitol. It is also clear, from the plots presented in the text, that slower cooling allows for more consistent results with fewer oscillations. However, the thermal resistance inside the phase change material is much higher than on the outside of the tubes, so the rate at which charging and discharging takes place are not influenced by the flow rate of the circulating oil around the tubes encapsulating the material

The effects of natural convection currents are important as they predominate after the melting of the material and consequently increase the heat transfer coefficients within the phase change material.

Acknowledgements

The authors are thankful to the project SHIP (Compete 2020 and Portugal 2020) for the financial support of this work. The experiments were carried out at the laboratory of INEGI—Instituto de Ciência e Inovaçãoem Engenharia Mecânica e Engenharia Industrial, an interface institute from the Faculty of Engineering of the University of Porto, Portugal.

Conflicts of Interest

The authors declare no conflicts of interest regarding the publication of this paper.

References

[1] Fleischer, A.S. (2015) Thermal Energy Storage Using Phase Change Materials Fundamentals and Applications. Springer, Minneapolis.

[2] Bruno, F., Belusko, M., Liu, M. and Tay, N.H.S. (2015) Using Solid-Liquid Phase Change Materials (PCMs) in Thermal Energy Storage Systems. In: Cabeza, L.F., Ed., *Advances in Thermal Energy Storage Systems*, Woodhead Publishing, Sawston, 201-246. https://doi.org/10.1533/9781782420965.2.201

[3] Ganatra, Y., Ruiz, J., Howarter, J.A. and Marconnet, A. (2018) Experimental Investigation of Phase Change Materials for Thermal Management of Handheld Devices. *International Journal of Thermal Sciences*, **129**, 358-364. https://doi.org/10.1016/j.ijthermalsci.2018.03.012

[4] Lin, Y., Alva, G. and Fang, G. (2018) Review on Thermal Performances and Applications of Thermal Energy Storage Systems with Inorganic Phase Change Materials. *Energy*, **165**, 685-708. https://doi.org/10.1016/j.energy.2018.09.128

[5] Nazir, H., Batool, M., Bolivar Osorio, F.J., Isaza-Ruiz, M., Xu, X., Vignarooban, K., Inamuddin, P.P. and Kannan, A.M. (2019) Recent Developments in Phase Change

Materials for Energy Storage Applications: A Review. *International Journal of Heat and Mass Transfer*, **129**, 491-523. https://doi.org/10.1016/j.ijheatmasstransfer.2018.09.126

[6] Fallahi, A., Guldentops, G., Tao, M., Granados-Focil, S. and Van Dessel, S. (2017) Review on Solid-Solid Phase Change Materials for Thermal Energy Storage: Molecular Structure and Thermal Properties. *Applied Thermal Engineering*, **127**, 1427-1441. https://doi.org/10.1016/j.applthermaleng.2017.08.161

[7] Crespo, A., Barreneche, C., Ibarra, M. and Platzer, W. (2019) Latent Thermal Energy Storage for Solar Process Heat Applications at Medium-High Temperatures—A Review. *Solar Energy*, **192**, 3-34. https://doi.org/10.1016/j.solener.2018.06.101

[8] Öztürk, H.H. (2005) Experimental Evaluation of Energy and Exergy Efficiency of a Seasonal Latent Heat Storage System for Greenhouse Heating. *Energy Conversion and Management*, **46**, 1523-1542. https://doi.org/10.1016/j.enconman.2004.07.001

[9] Solé, C., Medrano, M., Castell, A., Nogués, M. and Cabeza, L. (2007) Energetic and Exergetic Analysis of a Domestic Water Tank with Phase Change Material. *International Journal of Energy Research*, **31**, 135-147.

[10] Sioshansi, R. and Denholm, P. (2010) The Value of Concentrating Solar Power and Thermal Energy Storage. *IEEE Transactions on Sustainable Energy*, **1**, 173-183. https://doi.org/10.1109/TSTE.2010.2052078

[11] Nithyanandam, K. and Pitchumani, R. (2014) Cost and Performance Analysis of Concentrating Solar Power Systems with Integrated Latent Thermal Energy Storage. *Energy*, **64**, 793-810. https://doi.org/10.1016/j.energy.2013.10.095

[12] Zhang, H., Baeyens, J., Cáceres, G., Degrève, J. and Lv, Y. (2016) Thermal Energy Storage: Recent Developments and Practical Aspects. *Progress in Energy and Combustion Science*, **53**, 1-40. https://doi.org/10.1016/j.pecs.2015.10.003

[13] Khan, Z., Khan, Z. and Ghafoor, A. (2016) A Review of Performance Enhancement of PCM Based Latent Heat Storage System within the Context of Materials, Thermal Stability and Compatibility. *Energy Conversion and Management*, **115**, 132-158. https://doi.org/10.1016/j.enconman.2016.02.045

[14] Esteves, L.P., Magalhães, A., Ferreira, V. and Pinho, C. (2017) Evolution of Global Heat Transfer Coefficient on PCM Energy Storage Cycles. *Energy Procedia*, **136**, 188-195. https://doi.org/10.1016/j.egypro.2017.10.318

[15] Esteves, L., Magalhães, A., Ferreira, V. and Pinho, C. (2018) Test of Two Phase Change Materials for Thermal Energy Storage. Determination of the Global Heat Transfer Coefficient. *ChemEngineering*, **2**, 10. https://doi.org/10.3390/chemengineering2010010

[16] Trindade, J., Magalhães, A., Ferreira, V. and Pinho, C. (2018) Temperature Evolution Inside a Capsule Containing Phase Change Material. *ENCIT* 2018-17*th Brazilian Congress of Thermal Sciences and Engineering*, Águas de Lindóia, 25-28 November 2018. https://doi.org/10.26678/ABCM.ENCIT2018.CIT18-0065

[17] Rocha, T., Ferreira, V., Magalhães, A. and Pinho, C. (2020) Some Heat Transfer Data for a D-mannitol Derived Phase Change Material. *Renewable Energy and Power Quality Journal*, **18**, 18-23. https://doi.org/10.24084/repqj18.204

[18] Trhlikova, L., Zmeskal, O., Prikryl, R. and Florian, P. (2015) Thermal Properties of D-mannitol Derivative. *Advanced Materials Research*, **1126**, 181-186. https://doi.org/10.4028/www.scientific.net/AMR.1126.181

[19] Oró, E., Gil, A., Miró, L., Peiró, G., Álvarez, S. and Cabeza, L.F. (2012) Thermal Energy Storage Implementation Using Phase Change Materials for Solar Cooling and Refrigeration Applications. *Energy Procedia*, **30**, 947-956.

https://doi.org/10.1016/j.egypro.2012.11.107

[20] Solé, A., Neumann, H., Niedermaier, S., Martorell, I., Schossig, P. and Cabeza, L.F. (2014) Stability of Sugar Alcohols as PCM for Thermal Energy Storage. *Solar Energy Materials and Solar Cells*, **126**, 125-134. https://doi.org/10.1016/j.solmat.2014.03.020

[21] Rodríguez-García, M.M., Bayón, R. and Rojas, E. (2016) Stability of D-mannitol upon Melting/Freezing Cycles under Controlled Inert Atmosphere. *Energy Procedia*, **91**, 218-225. https://doi.org/10.1016/j.egypro.2016.06.207

[22] Bayón, R. and Rojas, E. (2017) Feasibility Study of D-D-mannitol as Phase Change Material for Thermal Storage. *AIMS Energy*, **5**, 404-424. https://doi.org/10.3934/energy.2017.3.404

[23] Gasia, J., Martin, M., Solé, A., Barreneche, C. and Cabeza, L.F. (2017) Phase Change Material Selection for Thermal Processes Working under Partial Load Operating Conditions in the Temperature Range Between 120 and 200˚C. *Applied Sciences*, **7**, 722. https://doi.org/10.3390/app7070722

[24] Pereira da Cunha, J. and Eames, P. (2016) Thermal Energy Storage for Low and Medium Temperature Applications Using Phase Change Materials—A Review. *Applied Energy*, **177**, 227-238. https://doi.org/10.1016/j.apenergy.2016.05.097

[25] Haillot, D., Bauer, T., Kröner, U. and Tamme, R. (2011) Thermal Analysis of Phase Change Materials in the Temperature Range 120-150˚C. *Thermochimica Acta*, **513**, 49-59. https://doi.org/10.1016/j.tca.2010.11.011

[26] Adipure Datasheet (2022) Adi-Pure High Purity Adipic Acid. https://adi-pure.invista.com/e-trolley/page_11546/index.html

[27] Ferrer, G., Solé, A., Barreneche, C., Martorell, I. and Cabeza, L.F. (2015) Corrosion of Metal Containers for Use in PCM Energy Storage. *Renewable Energy*, **76**, 465-469. https://doi.org/10.1016/j.renene.2014.11.036